# UAV Data Upscaling for Soil Erosion Monitoring in High-Latitude Rangelands, Northeastern Iceland

by

#### Sebastian Yerex

A graduating thesis submitted in partial fulfillment of the requirements for the Honours degree of Bachelor of Science

In the department of Geography

University of Victoria 2024

We acknowledge and respect the ləkwəŋən (Songhees and Esquimalt) peoples on whose traditional territory UVic stands, and the ləkwəŋən and WSÁNEĆ peoples whose historical relationships with the land continue to this day.

#### **Abstract**

Soil erosion, while a typical geomorphic process, can be amplified and accelerated by land use and climate change. In Iceland, changes in vegetation cover since settlement in the 9th century have led to increased soil erosion. Current field-based methods for erosion mapping and monitoring are difficult and costly to employ frequently and over large regions. The systematic and synoptic nature of satellite remote sensing is well-suited for wide-scale environmental monitoring. However, fine-scaled erosional features may be obscured in coarse and moderate-resolution imagery (30-10 m). Here the synergistic use of RGB uncrewed aerial vehicle (UAV) and multispectral Sentinel-2 as well as field-based data, in the form of existing land monitoring data and quadrats for validation, is examined to bridge the gap between ground-based and spaceborne monitoring in northeastern Iceland. High resolution (< 5cm) land cover maps from UAV imagery are produced with a random forest (RF) classifier, for six sites. Field validation shows high overall accuracy (> 90%). These data are upscaled to build a RF regression model estimating bare soil cover, yielding good results ( $R^2 = 0.814$ ). Using governmental land-monitoring data (GroLind), erosion severity classes are defined and a map for a portion of northeastern Iceland is produced. This study highlights the potential of multiscale remote sensing for estimating sub-pixel landscape information relevant to environmental monitoring in tundra environments.

**Supervisory Committee** 

Dr. Noémie Boulanger-Lapointe, Supervisor Department of Geography

Dr. Sophie Norris, Second Reader Department of Geography

# **Table of contents**

Abstract	i
Table of contents	ii
Acknowledgments	iii
1.0 Introduction	1
2.0 Materials and Methods	5
2.1 Study site	5
2.2 Data	6
2.2.1 UAV data	6
2.2.2 Quadrat data	8
2.2.3 Sentinel-2 data	10
2.2.4 Field validation data	10
2.3 Fractional vegetation cover	11
2.3.1 Vegetation indices.	11
2.3.2 UAV-scale classification	13
2.3.3 Upscaling.	14
2.4 Satellite-scale model.	14
2.4.1 Satellite vegetation indices.	14
2.4.2 Regression model	15
2.5 Erosion severity	16
3.0 Results	17
3.1 UAV-scale classification.	17
3.2 Upscaling UAV data	17
3.3 Satellite regression and erosion severity	19
4.0 Discussion	21
4.1 UAV-scale classification	22
4.2 Upscaling and satellite scale mapping	23
4.3 Future work	
5.0 Conclusion	26
6.0 References	27
A nu on dier	26

## Acknowledgments

First and foremost, I would like to thank my supervisor, Dr. Noémie Boulanger-Lapointe, for the valuable support, guidance, and opportunities she has offered me throughout the final two years of my undergraduate degree. Dr. Boulanger-Lapointe has facilitated the highest achievements of my degree and her constant belief in me throughout this project has allowed me to push myself and develop as a researcher. I would also like to express my gratitude to my second reader Dr. Sophie Norris, for her thoughtful feedback and questions on my thesis and during my oral defense.

I am indebted to Marteinn Möller for his hospitality while I stayed in Iceland, for allowing me to join along on his field work, and for allowing me to use his UAV data for this project. Without Marteinn's kindness and generosity this project would not have been possible, it was a pleasure to meet and work with him

I am grateful for all the funding that has allowed me to conduct this research, Polar Knowledge Canada: Northern Scientific Training Program (NSTP); the University of Iceland; the University of Victoria: Jamie Cassels Undergraduate Research Award (JCURA) and the Ross Fund. Thank you to the Soil Conservation Service of Iceland for allowing me access to their field data, and thank you to Resource International for their In-Kind contributions.

Finally, my special thanks to my friends and family, especially Lindsay, Tony, Gemma, and my Mom. Their non-stop love, support, understanding, and humor has helped me through every challenge, I am endlessly grateful to all of them.

#### 1.0 Introduction

Soil erosion is a geomorphic process through which soil particles (sediments, soil aggregates, and organic matter) are entrained and transported away from their primary location (Poesen, 2018). Through intense erosion, soils become less fertile as nutrients are removed (O. Arnalds et al., 2001). Natural erosive processes such as rain, wind, and gravity as well as biological processes including trampling and burrowing by wildlife are typical in most landscapes (Poesen, 2018). Anthropogenically induced changes in land use and climate however, can amplify and accelerate erosion beyond the capability of an ecosystem to generate new soil, causing rapid landscape degradation (Borrelli et al., 2021; Poesen, 2018).

Vegetation cover has a strong influence on the rate and severity of soil erosion (Durán Zuazo et al., 2008; Gyssels et al., 2005). Vegetation can shield erosion prone soil from wind and precipitation as well as provide support against gravity on slopes, limiting soil loss (Tang et al., 2021). Vegetation composition, structure, and coverage is changing in many high latitude regions due to climate change and other anthropogenic pressures. The exact nature of these changes however and their impact on soil erosion is complex and not well understood (Myers-Smith et al., 2020; Streeter & Cutler, 2020). In order to better understand this change and effectively target restoration and mitigation efforts, monitoring of vegetation cover and soil erosion change must be improved.

Iceland has experienced rapid and severe landscape degradation since human settlement in the 9th century, including dramatic loss in vegetation and increase in soil erosion (O. Arnalds, 2015;

Dugmore et al., 2009; Greipsson, 2012; Ólafsdóttir et al., 2001). This is particularly true for the highland region which encompasses remote wilderness areas above the potential treeline (approx. 200-400 m a.s.l (Boulanger-Lapointe et al., 2022)), where sub-alpine tundra vegetation are dominant (Thórhallsdóttir, 1997). Grazing pressure increased dramatically in the highlands with animal husbandry accompanying human settlement, ~11,00 years ago (McGovern et al., 2007). The highlands are most sensitive to this change due to the short growing season and disturbance from glacial and volcanic activity (Ó. Arnalds et al., 2023; Dugmore et al., 2009). Disturbed vegetation in this region is slow to recover, leaving soil exposed to further disturbance (Figure 1 & 2). The soils found in much of the highlands tend to lack strong cohesive properties and are easily entrained by frequent, strong winds (O. Arnalds, 2015). The result is the poor land conditions seen in many parts of Iceland today, with over 39% of the country's total area considered to be eroded as of 2001 (O. Arnalds et al., 2001; Ó. Arnalds et al., 2023).

Currently, the main source of erosion data for Iceland comes from a series of maps produced Between 1991 and 1997. During this time the Agricultural Research Institute (ARI) and Soil Conservation Service (SCS) of Iceland used field observations and manual interpretation of Landsat 5 imagery to map erosion severity across the country. The project produced coarse resolution products categorizing erosion severity into 6 classes (0-5) (O. Arnalds et al., 2001; O. Arnalds, 2015). This mapping provided critical quantification of land conditions on a wide scale. However, in the 27 years since these maps were produced it is likely that land conditions have changed in many regions. This includes both the progression and regression of soil erosion. As such the ability to accurately examine and analyze current land conditions using these maps is limited (Ó. Arnalds et al., 2023).

Satellite imagery and machine learning are important tools that have improved the accuracy and efficiency of many monitoring and mapping tasks including those related to soil erosion (Sepuru & Dube, 2018). Such tools have been applied to regions of Iceland in previous studies.

Fernández et al., 2022 highlights the potential of remote sensing for this application, using Sentinel-2 imagery alongside topographic data to predict erosion risk from field observations of erosion severity provided by the SCS. While the results show good accuracy, nuanced information is lost in the broad 6-point classification scheme and physical attributes important to management such as vegetation cover cannot be interpreted from the results.

It has been common for the Normalized Vegetation Index (NDVI) to be used as a proxy for vegetation cover. NDVI takes advantage of the divergent spectral response of green vegetation in the red and near infrared (NIR) portions of the electromagnetic spectrum. In simple terms, high NDVI are interpreted as indicating dense, healthy green vegetation. Low NDVI values are interpreted as indicating the lack of vegetation and therefore the relative dominance of bare surface cover (Hurcom & Harrison, 1998; Xiao & Moody, 2005).

While NDVI can be well correlated with vegetation cover this is not always the case (Ayalew et al., 2020; Laidler et al., 2008). Changing climate in the arctic, which drives change in vegetation composition, further breaks down this relationship. In particular the increase in tundra shrub communities is thought to inflate the near infrared (NIR) portion of an area's spectral profile (Juszak et al., 2014). Therefore if a positive relationship between shrub abundance and NDVI is seen; this relationship may mask eroded areas (Kodl et al., 2024). Other vegetation indices (VIs)

have shown promise in determining vegetation cover and previous studies suggest that these VIs should be considered in addition to NDVI (Riihimäki et al., 2019). Furthermore, other VIs show better sensitivity compared to NDVI for tundra species, especially VIs using red-edge (RE) bands (Buchhorn et al., 2013; Liu et al., 2017).

Adding further complication is the aggregation of spectral information in coarse resolution remote sensing products (i.e Sentinel-2 satellite imagery). This information loss is a particularly important consideration in arctic tundra landscapes, where many processes contribute to high heterogeneity in landscape features (Virtanen & Ek, 2014). Vegetation and land cover can be highly spatially variable. Uncrewed aerial vehicles (UAVs) can produce very high resolution imagery and continue to become more accessible and adopted by the research and management communities. There are various ways in which UAV and satellite data can be used synergistically. One approach is the calibration of satellite data or models acting on satellite data using UAV data, often termed upscaling (Alvarez-Vanhard et al., 2021).

UAV data upscaling has been shown as an effective method for model calibration in fractional land cover problems relating to tundra and similarly heterogeneous landscapes (Bergamo et al., 2023; Riihimäki et al., 2019). By applying machine learning at multiple scales, linked through spatial aggregation, the dominance of sub-pixel physical characteristics can be estimated. Examples of UAV upscaling previous applications include mapping fractional coverage of invasive shrub species in northern Estonia and forage lichen in northern Canada (Bergamo et al., 2023; Fraser et al., 2022). For vegetation related problems NIR coverage is particularly important due to the prominent spectral signature of vegetation related to plant cell structure and

pigments (Knipling, 1970). While UAVs mounted with multispectral cameras, which have NIR coverage, are increasingly accessible they remain less common and more costly than those mounted with RGB cameras. Multispectral based classifications tend to produce higher accuracy results compared to RGB based classifications. However, RGB based classifications from UAV data often produce good accuracy (> 90%) (Fraser et al., 2022).

The aim of this study is to examine the integration of UAV and satellite data, through upscaling, as a means for estimating bare soil cover for soil erosion monitoring. This is accomplished by classifying UAV imagery to extract bare soil, which provides training data for a satellite-scale regression model estimating fractional bare soil cover. These data are combined with existing land monitoring information to classify soil erosion severity.

#### 2.0 Materials and Methods

#### 2.1 Study site

The study was conducted at six sites located in northeastern Iceland (Figure 1). Sites were randomly chosen in the Múlaþing and Norðurþing areas of the highlands, above 400m elevation (Ó. Arnalds et al., 2023). All sites are located within open sheep grazing commons (O. Arnalds & Barkarson, 2003). The Möðrudalur weather station nearby shows a mean annual temperature of 0.5 °C and mean annual precipitation of 348.6 mm from 1960 to 2007 as well as a mean annual wind speed of 5.5 m s<sup>-1</sup> from 1981 to 2007 (Icelandic Meteorological Office, 2012). Vegetation types in the region are a mix of heath, grasslands, moss heaths and wetlands (Kardjilov et al., 2006). The UAV survey sites encompass a range of erosion severity, from fully

vegetated to severely eroded areas (O. Arnalds et al., 2001). Soils in the region are primarily Andosolic and Virtisolic (O. Arnalds, 2015; O. Arnalds & Óskarsson, 2009)

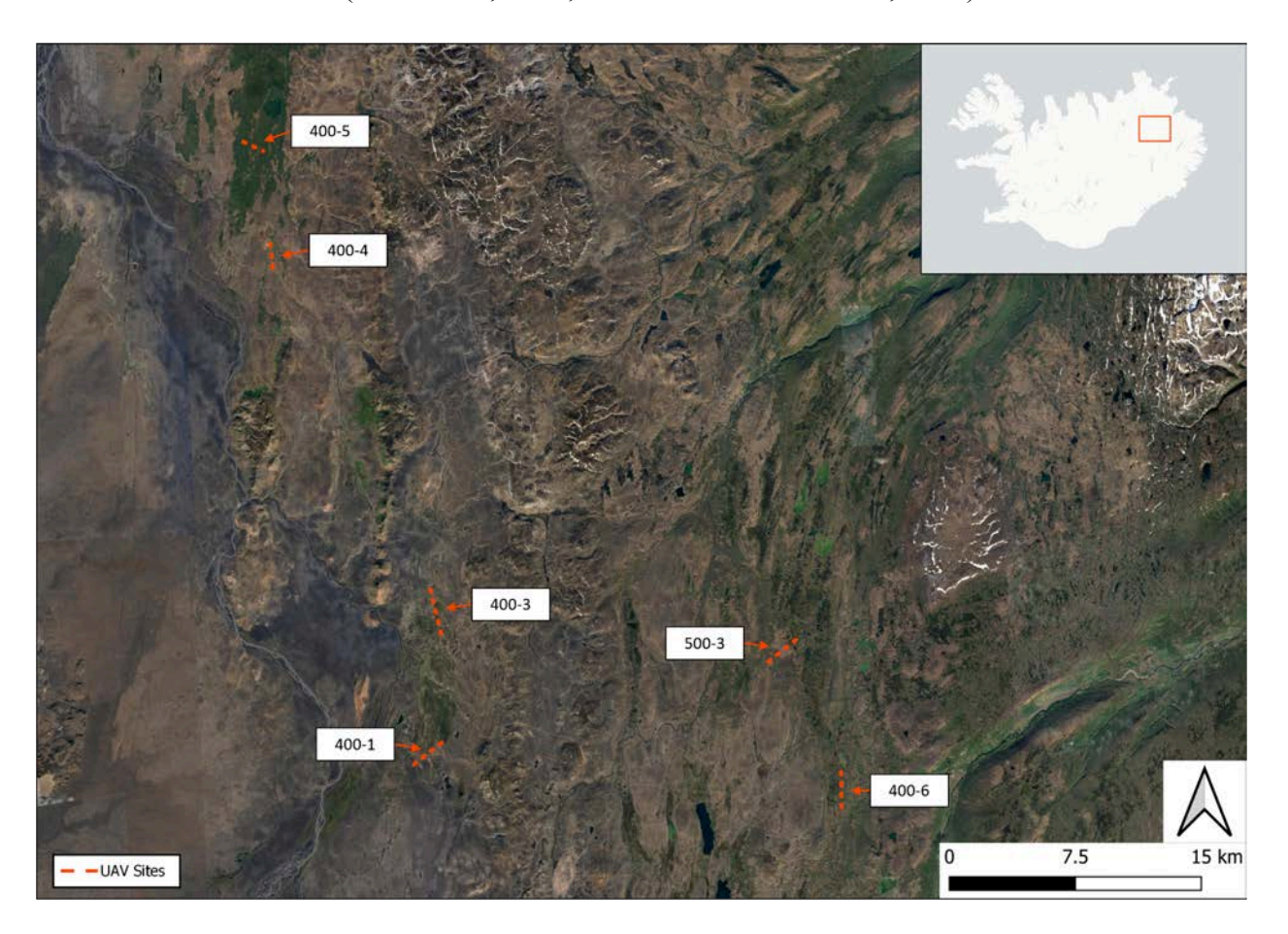


Figure 1: Location of UAV survey sites, northeastern Iceland. Survey sites marked with orange dashed lines.

# 2.2 Data

# 2.2.1 UAV data

In July 2023, imagery was collected along six 1.4 - 3.1 km transects in eastern Iceland, using the RGB sensor onboard a DJI Mavic 3T quadcopter UAV. The red band has a wavelength of 650 nm ( $\pm 16$  nm) the green 560 nm ( $\pm 16$  nm) and the blue 450 ( $\pm 16$  nm).



Figure 2: An oblique UAV image showing partially eroded landscape, northeastern Iceland.

The UAV was flown at approximately 80 m above ground level. Images were set to capture with 80% front overlap. The width of each transect was approximately 60 m. Best attempts were made to coordinate flights at similar times relative to solar noon, however due to weather conditions and time constraints this was largely not possible and periods of up to 5 hours separate the capture times between sites. The long daylight hours at this time of year in high-latitude regions however minimized differences in the amount of illumination.

The UAV data were processed in Agisoft Metashape version 2.1.0. Photogrammetric processing was applied following the recommended steps from the software developers (Agisoft LLC., St. Petersburg, Russia). Images containing excessive motion blur were removed prior to processing. Georeferencing was based on the GPS unit and internal measurement unit onboard the UAV, producing an estimated horizontal positioning error of ~3m. This process produced a single orthomosaic for each of the six transects with spatial resolutions of 4-5 cm.

## 2.2.2 Quadrat data

Prior to each UAV flight 10 randomly selected points along each transect were overlaid with a 50 cm-by 50 cm quadrat. An image of each quadrat placement was taken at waist height (~105 cm) with a digital camera (Figure 3) and the percent bare soil within the quadrat was recorded. The center of each quadrat was marked with a flag, for identification in the UAV imagery, and the location was recorded with a Garmin Etrex 10 handheld GPS unit.

This data was used to examine the agreement between field observations and the UAV classification of percent bare soil. The coordinate of each quadrat placement was used to find the corresponding flag in each orthomosaic. A 50 cm-by-50 cm polygon was drawn around the flag, using the corresponding field photograph to inform polygon delimitation. Percent bare soil within the polygon was found by counting the number of pixels classified as bare soil in the UAV-scale classification, using the zonal histogram tool in QGIS v3.28 (QGIS Development Team, 2009). This value was then divided by the total number of pixels within the polygon and multiplied by 100 (Riihimäki et al., 2019). The data was evaluated by calculating the Root Mean Square Error (RMSE).

$$RMSE = \sqrt{\frac{\sum_{i=1}^{n} (\hat{y}_i - y_i)^2}{n}}$$

Where  $\hat{y}_i$  is the classification based estimate and  $y_i$  is the observed value from the field.

Due to human error in the field the quadrat points for sites 400-4 and 400-5 fell outside of the UAV imagery. As a result quadrat based RMSE values for these two sites could not be calculated.

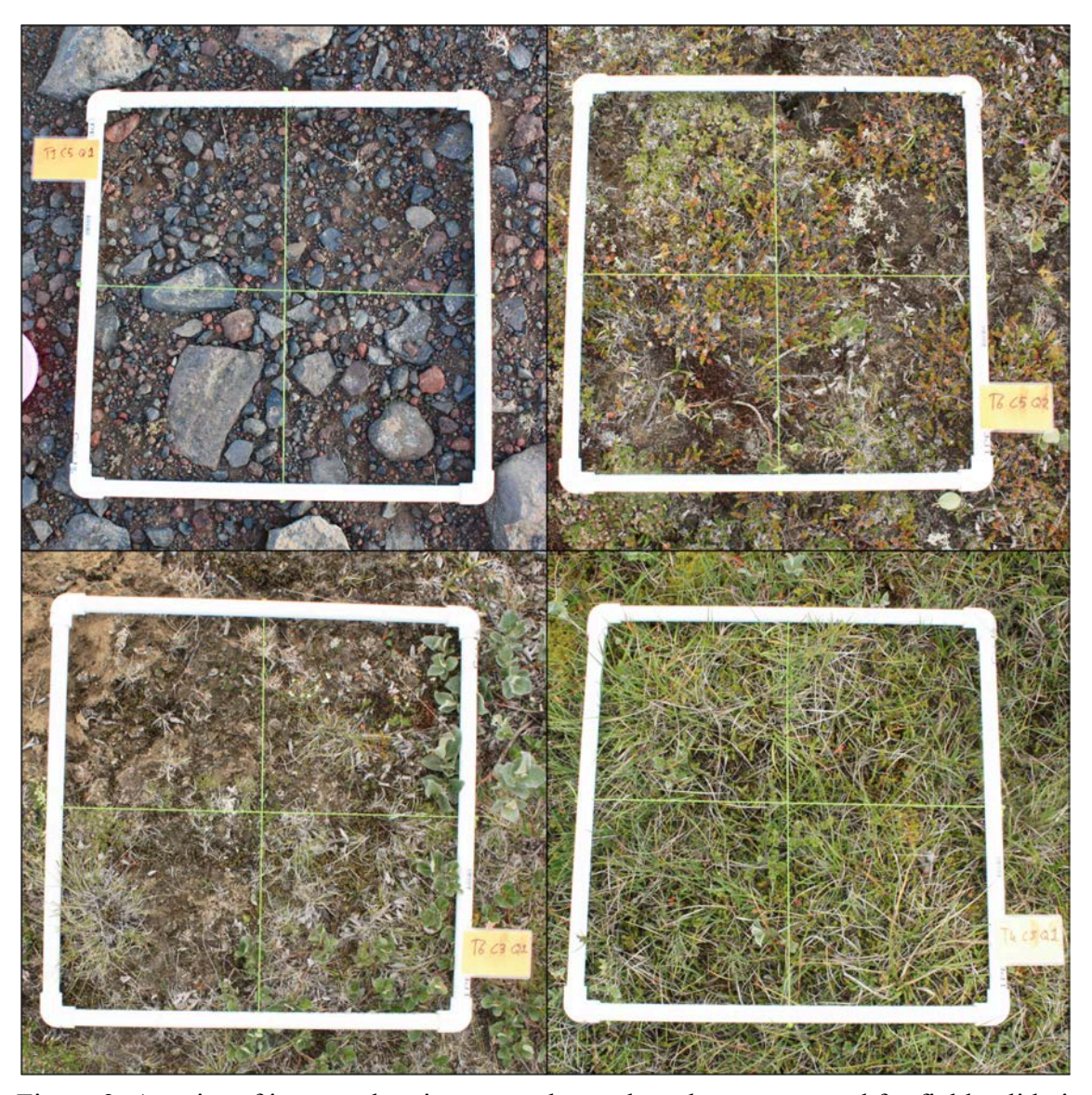


Figure 3: A series of images showing example quadrat placements used for field validation of the

UAV-scale classification.

#### 2.2.3 Sentinel-2 data

Service, using the Advanced Temporal Mosaic tool. The temporal range was set to search data acquired between July 31, 2023 and August 31, 2023. The SEN2COR atmospheric correction method and ESA cloud mask options were used (Main-Knorn et al., 2017; *Sentinel-2 Global Mosaic Service*, 2014).

#### 2.2.4 Field validation data

GróLind is a land monitoring initiative from the Icelandic Soil conservation service. Part of the GróLind project is field observations at over 1000 marked sites. Each site consists of a 50 x 50 m plot containing two perpendicularly intersecting 50 m long belt transects. Approximately 200 sites are visited annually resulting in a five year revisit time for each site. At these sites variables relating to ecological status are recorded, including vegetation height, soil depth, soil type, and erosion rating (Marteinsdóttir et al., 2021). Here primary erosion severity and fractional vegetation coverage data from sites visited in 2019 were used to examine the relationship between field observed erosion severity and modeled bare soil cover.

# 2.3 Fractional vegetation cover

# 2.3.1 Vegetation indices

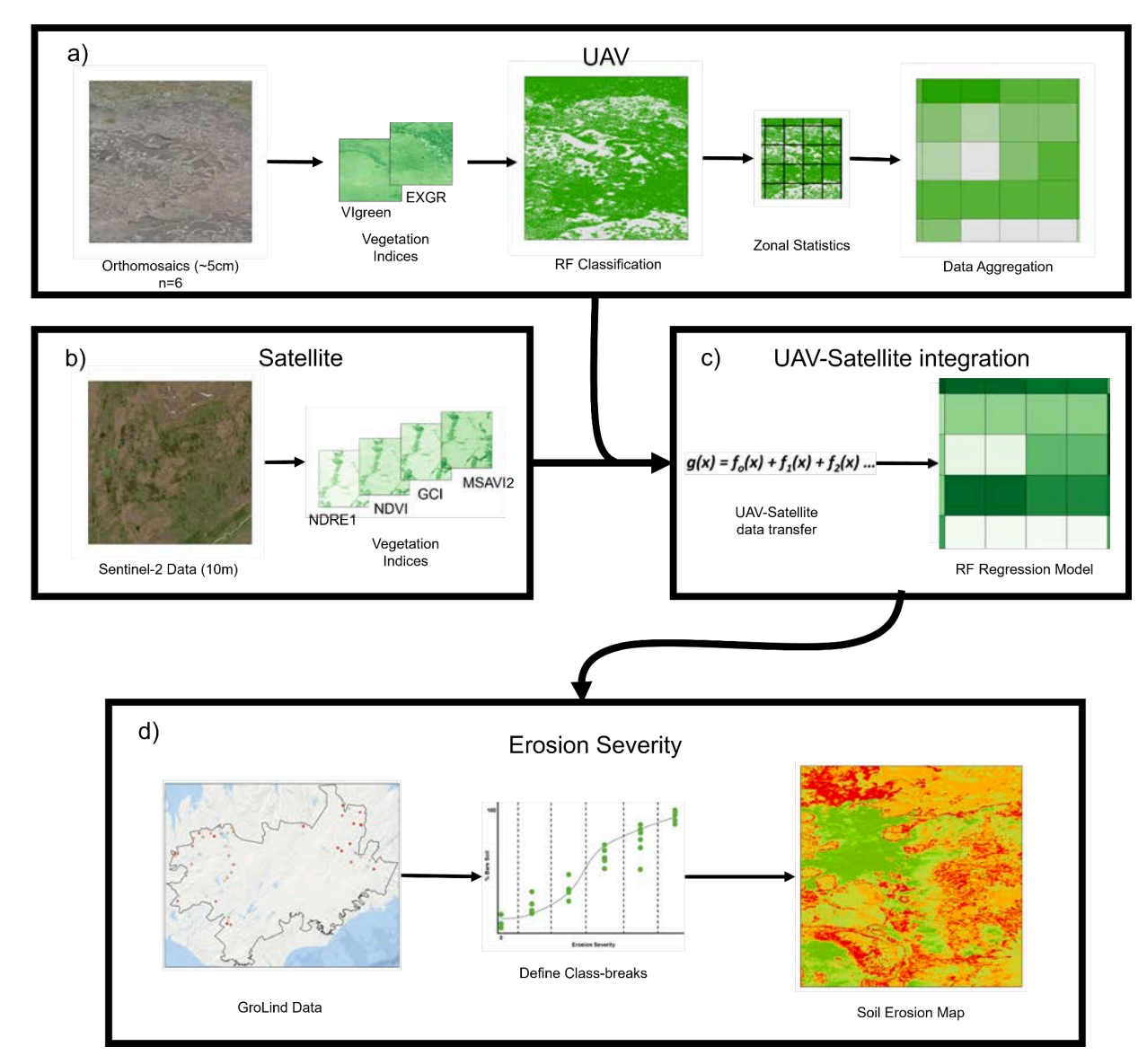


Figure 4: Workflow for UAV data upscaling and erosion severity mapping. a) UAV data treatment after preprocessing, b) Sentinel-2 satellite data treatment, c) UAV and Sentinel-2 satellite data integration, d) integration of GroLind data for erosion severity mapping.

The lack of an NIR band in the UAV data reduces the ease with which vegetation can be distinguished from background materials. This is because most vegetation strongly reflects in the NIR range and absorbs strongly in the visible range, for green vegetation the red range. This divergent signature is typically distinct from the background signature.

In order to provide more information to the UAV-scale model and improve vegetation and soil separability two RGB VIs were calculated using the *terra* package for R v4.2.2 (Hijmans, 2023; R Core Team, 2022). The two VIs: VIgreen and EXGR, were selected based on their ability to effectively separate bare soil and vegetation, demonstrated in a previous study (Vieira & Rodrigues, 2021). To calculate these VIs the RGB data was first normalized using a two-step process (Guijarro et al., 2011; Marcial-Pablo et al., 2019; Vieira & Rodrigues, 2021).

i)

$$R_n = \frac{R}{R_{max}} G_n = \frac{G}{G_{max}} B_n = \frac{B}{B_{max}}$$

Where R, G, B are the values in the original red, green, and blue channels of the UAV data, respectively.  $R_{max}$ ,  $G_{max}$ , and  $B_{max}$  are the maximum values of the original 8-bit channels (255).

$$r = \frac{R_n}{R_n + G_n + B_n} g = \frac{G_n}{R_n + G_n + B_n} b = \frac{B_n}{R_n + G_n + B_n}$$

Where r, g, and b are the normalized spectral components.

With the normalized data the VIs were calculated as follows (Gitelson et al., 2002; Meyer & Neto, 2008).

$$VIgreen = \frac{g-r}{g+r}$$

$$EXGR = (2g - r - b) - (1.4r - g)$$

## 2.3.2 UAV-scale classification

For the UAV-scale classification training and validation data were generated for 5 class types: bare soil (dark), bare soil (light), green vegetation, non-green vegetation, and water (for examples see Figure A1). The goal of using these classes rather than a binary bare soil presence-absence scheme was to reduce error by providing narrow classes with less variation in spectral signature. Along each transect 10, 50cm-50cm polygons were manually delineated for each class, in QGIS, resulting in 50 polygons per transect. The location of the polygons was determined by examining the RGB orthomosaics, selecting areas of homogeneous, class representative cover.

The two VIs, each of the normalized RGB bands, and the raw orthomosaic RGB bands were used as predictive variables. Each pixel within the polygons (~360 per polygon) were sampled to extract values for these variables. This provided approximately 18,000 sampled points per transect. These data were split randomly into training (70%) and validation (30%) sets, using a stratified approach to ensure an equal number of training and validation points between the five classes.

A RF classification model was implemented using the *caret* and *randomForest* packages in R (Kuhn & Max, 2008; Liaw & Wiener, 2002). RF was chosen based on the accuracy of the model for classifying land cover from RGB UAV imagery demonstrated in previous studies (Bergamo et al., 2023; Fraser et al., 2022). An individual model was fit for each transect to improve site-specific accuracy due to the previously mentioned variation in illumination conditions (Kodl

et al., 2024). A 10-fold cross-validation was used. The number of variables to randomly sample at each split, a parameter known as mtry, was optimized using a grid search, testing values between 1 and 8. The number of trees was set to a constant of 500. A confusion matrix was produced for each site using the validation data, accuracy and Kappa values were used to assess model performance. The model with optimal parameterization for each site was applied to a stack of raster layers containing the eight variables.

## 2.3.3 Upscaling

To upscale the UAV-scale classification a within-pixel coverage method was used to find percent bare soil (Bergamo et al., 2023; Riihimäki et al., 2019). A grid was generated directly from the Sentinel-2 data to match the 10 m spatial resolution. Segments of this grid were clipped to match the extent of each transect. The zonal histogram tool in QGIS was used to compute the number of pixels in the UAV-scale classification assigned to each of the five classes, within each grid cell. The two bare soil classes were merged and compared to the occurrence of the remaining classes within each grid cell to determine the percent bare soil coverage (0-100).

## 2.4 Satellite-scale model

## 2.4.1 Satellite vegetation indices

Similarly to the UAV-scale classification, satellite VIs provide more spectral information and can improve the separability of bare soil and vegetation. Here four VIs were derived from the Sentinel-2 data: GCI, MSAVI2, NDVI, and NDRE1. The first three VIs were selected based on the performance when previously applied to identify overgrazing hotspots (Harmse et al., 2022). The fourth VI was selected based on the potential shown in a previous study to identify bare soil

and performance in regions of low vegetation cover (Andreatta et al., 2022). These VIs were calculated as follows.

$$GCI = \frac{NIR}{Green} - 1$$

Where NIR and Green are Sentinel-2 bands 8 and 3, respectively.

$$MSAVI2 = \frac{2*NIR+1\sqrt{(2*NIR+1)^2-8(NIR-Red)}}{2}$$

$$NDVI = \frac{(NIR-Red)}{(NIR+Red)}$$

Where Red is Sentinel-2 band 4.

$$NDRE1 = \frac{(RE_{740} - RE_{705})}{(RE_{740} + RE_{705})}$$

Where  $RE_{740}$  and  $RE_{705}$  are Sentinel-2 bands 6 and 5, respectively. Sentinel-2 bands 5 and 6 are 20 m resolution and therefore were resampled to match the 10 m resolution of the remaining bands used.

# 2.4.2 Regression model

A point was placed at the center of each grid cell produced in the upscaling process. The calculated percent bare soil for each cell (see section 2.3.3) was then transferred to the corresponding point. The values from each of the Sentinel-2 variables, bands 2-8, and the four VIs were sampled at each point. This produced 18,287 data points. These data were split into training (70%) and validation (30%) sets.

A RF regression model was implemented on the training data using the *caret* and *randomForest* packages in R (Kuhn & Max, 2008; Liaw & Wiener, 2002). RF was chosen based on its accuracy in upscaling applications presented in previous studies (Fraser et al., 2022). A model fitting

procedure similar to that used for the UAV-scale classification model was used. A 10-fold cross validation was used. The mtry parameter was optimized using a grid search with values between 1 and 11. The number of trees was set to a constant of 500. The best model was chosen based on RMSE and R<sup>2</sup>. The best model was run on the validation set and the RMSE and R<sup>2</sup> were calculated to assess the models predictive performance. The final model was applied to a stack of raster layers containing the 11 variables.

# 2.5 Erosion severity

The GróLind data were subset to contain only points within the highlands region (above 400m elevation) leaving 76 sites. Two variables from these GróLind points were extracted. The first variable, primary erosion severity, ranked on a scale of one (little erosion) to five (extremely severe erosion). The second variable, fractional vegetation cover, ranked on a scale of one (0%) to five (100%). A Pearson correlation test was run on the two variables to establish if there is a significant relationship between the fractional vegetation cover and erosion severity as observed in the field. The results indicate a strong (0.82) significant (p-value < 0.005) relationship. A linear regression was fit to estimate erosion severity from bare soil cover within the GróLind data. The satellite-scale bare soil cover model was reclassified to the five-point fractional vegetation cover scale used in the GróLind data. The linear regression was then applied to this data to estimate soil erosion severity; non-whole values of erosion severity were reclassified to the nearest whole number in order to fit the five-point GróLind classification scheme (e.g. 1.5 → 2).

#### 3.0 Results

#### 3.1 UAV-scale classification

The random forest classifier produced an overall accuracy of 96.6% across all six sites with a Kappa of 0.95 and RMSE of 15.36% (Table 1). The best results were achieved at site 400-5, with an accuracy of 98.6% and Kappa of 0.98. The poorest results were achieved at site 400-3 with an accuracy of 92.2%, a Kappa of 0.90, and RMSE of 40.17%. Aside from site 400-3 all sites achieved accuracy greater than 95%, Kappa scores greater than 0.94, and RMSE less than 9%.

Table 1: Summary of the accuracy results for UAV-scale classification at each site and overall. accuracy and kappa based on cross validation, RMSE based on quadrat fractional coverage.

Site:	Accuracy (%):	Карра:	RMSE (%):
Overall	96.6	0.95	15.36
400-1	97.4	0.97	6.67
400-3	92.2	0.90	40.17
400-4	96.6	0.94	-
400-5	98.6	0.98	-
500-3	97.8	0.97	8.78
500-6	97.0	0.96	5.76

# 3.2 Upscaling UAV data

Figure 5 shows an example of the within-pixel fractional coverage aggregation used to upscale the UAV-scale classification results. Relatively large erosional features, where continuous areas of bare soil are exposed, are well represented in both the UAV classification and aggregated data.

Away from the center of these features exposed soil becomes fragmented and appears in smaller patches, as vegetation cover increases. This pattern is distinct in the UAV-scale classification results. Due to the aggregation inherent in the upscaling process however, this pattern is obscured as the resolution becomes much larger than individual erosional patches. While the aggregated data tend to show the pattern of increased vegetation with distance away from erosional features, the distribution of exposed soil within a cell is lost. A result of this is that the precise edge of an erosional feature can be difficult to discern at the aggregated scale. For example, if the edge of an erosional patch is outlined by dense vegetation the fractional coverage from the aggregated data may be low. The low bare soil coverage may not reflect the severity of erosion in that cell; this effect is highlighted in the annotated inset of Figure 5.

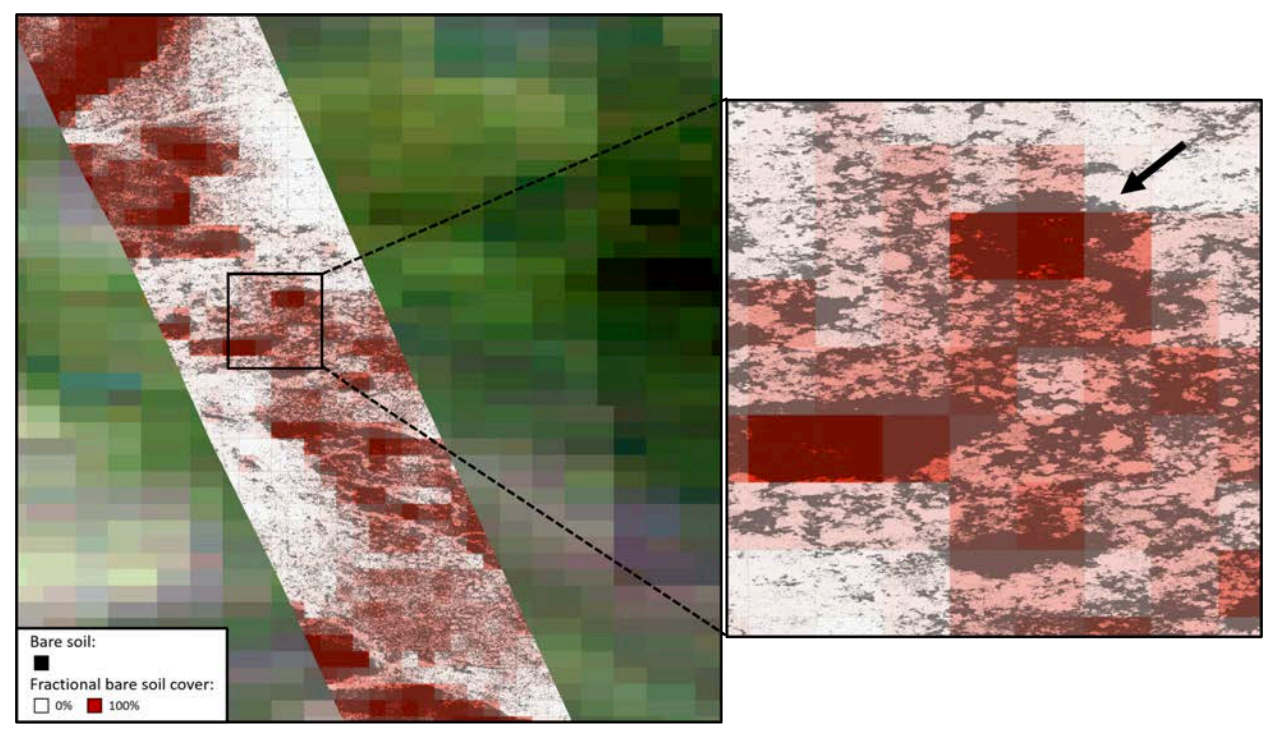


Figure 5: UAV-scale classification of bare soil shown in black (presence of bare soil), overlain with fractional bare soil coverage produced from aggregation during the upscaling process. Site 400-3. Black arrow on the left panel shows an example of an erosional feature edge being obscured due to aggregation.

# 3.3 Satellite regression and erosion severity

The satellite-scale percent bare soil cover regression model produced an  $R^2$  of 0.814, for all sites (Figure 6a). The site specific results show a wide range of  $R^2$  values. Site 400-1 (Figure 6b) produced the lowest  $R^2$  (0.403), showing a large number of points estimated to have a greater bare soil cover than classified in the UAV data. Site 500-3 produced the highest  $R^2$  (0.924).

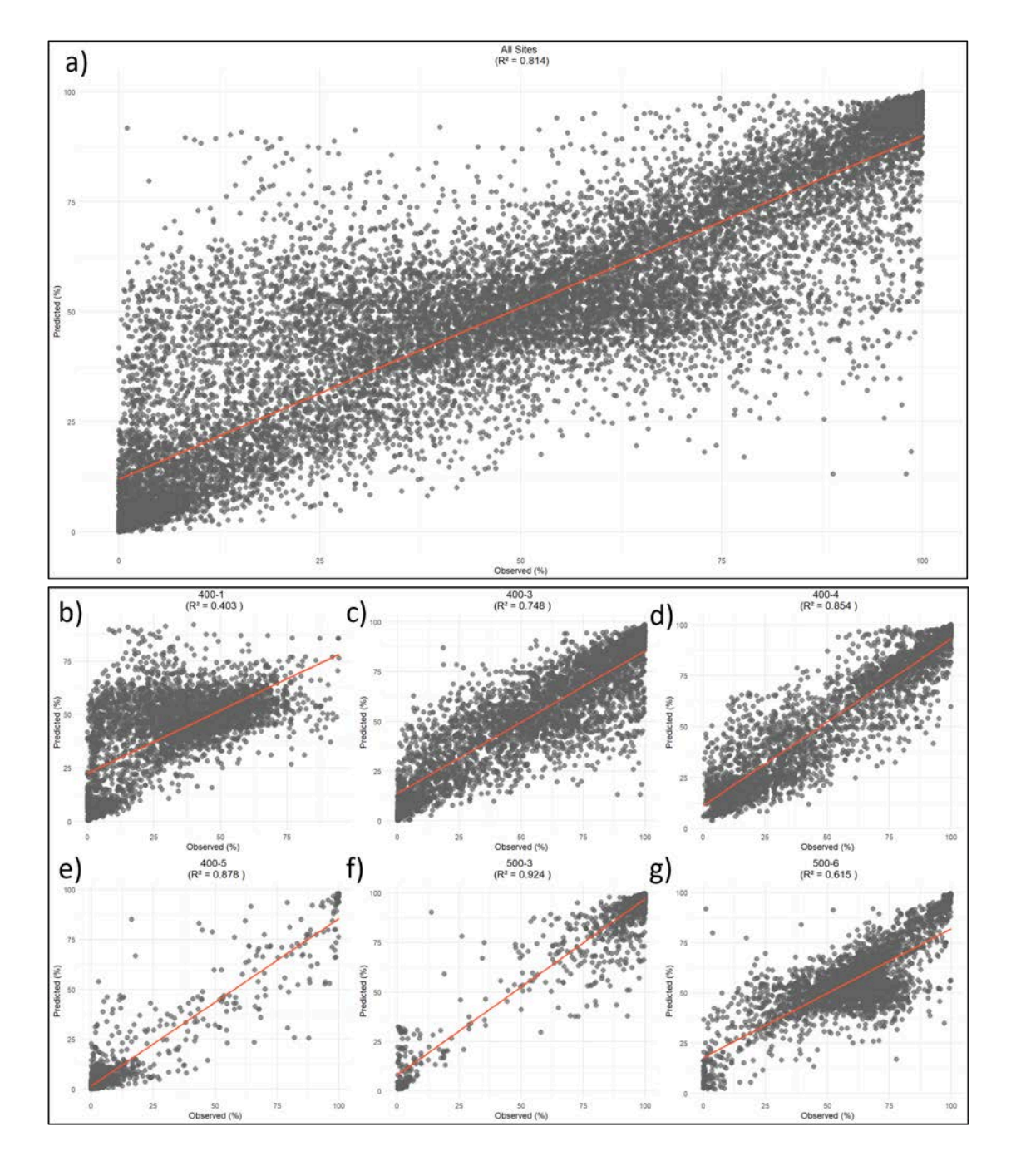


Figure 6: A series of scatter plots showing the percent bare soil coverage from the satellite-scale regression model (predicted) compared to the aggregated UAV-scale classification (observed), best fit line shown in orange. Top (a) panel shows the results for all six sites overall. Bottom (b-g) panel shows the results at each site.

Figure 7 shows the output bare soil cover (a) and erosion severity (b) maps produced through UAV data upscaling. The UAV sites largely avoid regions of very dark sands and gravel like those near site 400-4 and 400-5 (Figure 7c). In the bare soil cover map (Figure 7a) regions with this composition appear to have higher vegetation cover than expected. As a result the erosion severity assigned to these areas tends to be lower than anticipated.

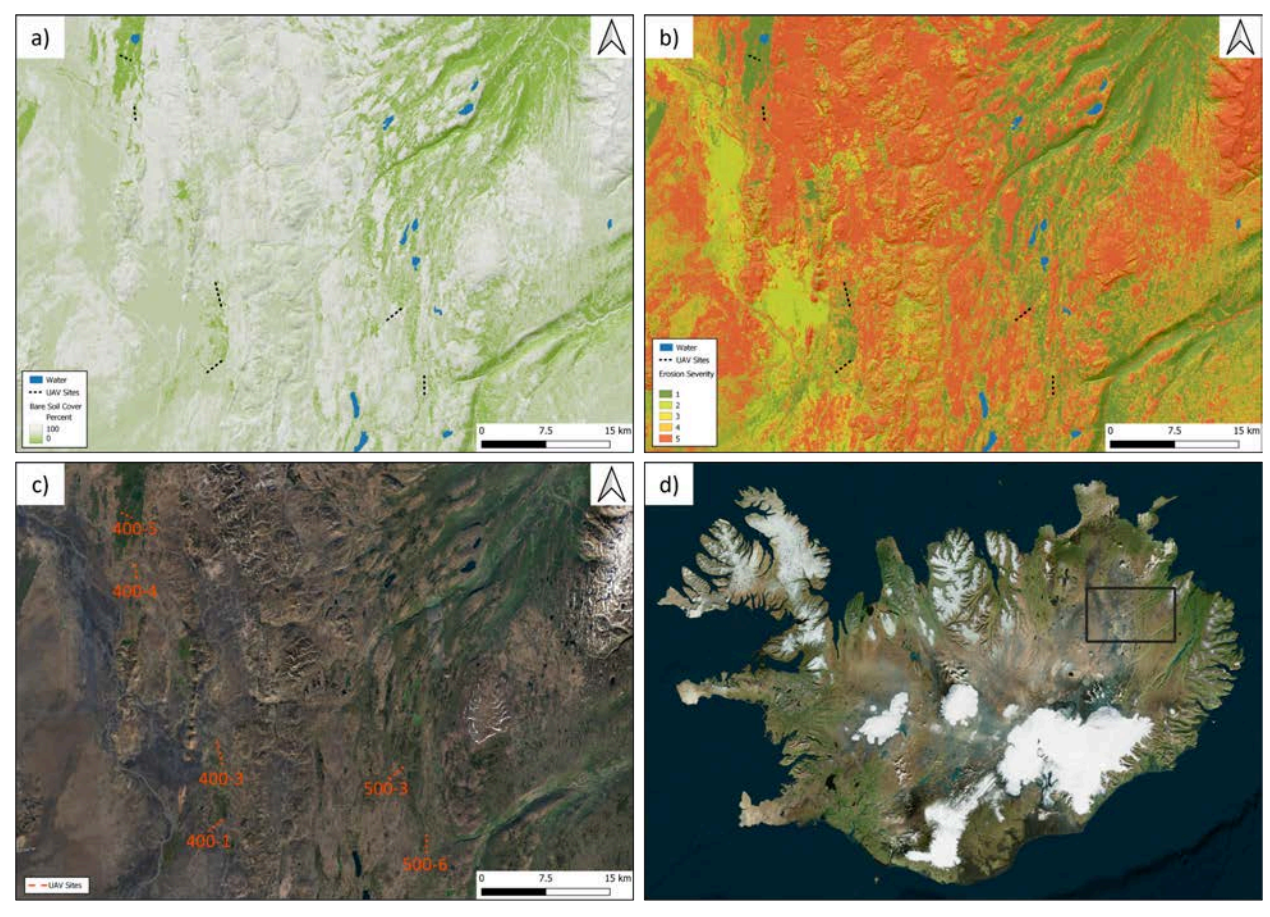


Figure 7: a) percent bare soil cover map from upscaled UAV data, b) erosion severity map from GroLind erosion severity data c) Sentinel-2 true color composite d) true color composite showing the extent of panels a-c.

# 4.0 Discussion

This study illustrates the potential of integrating UAV and satellite data to extract physical parameters, in this case bare soil cover, for mapping and monitoring soil erosion in tundra environments. The methods presented here show that UAV data upscaling with a RF regression model can provide continuous estimates of percent bare soil cover at the satellite pixel scale. The use of UAV data in this way could provide a cost-effective alternative to on-foot field measurements and produce high quality training data for semi-automated mapping from satellite

imagery. Parameters upscaled from UAV data can be integrated with existing soil erosion data to expand the scope beyond measured locations (Bergamo et al., 2023).

## 4.1 UAV-scale classification

The UAV-scale RF classifications based on RGB VI's were able to separate bare soil and vegetation with accuracies comparable to multispectral UAV based classifications (Furukawa et al., 2021). The use of multiple VI's and a five class scheme improves upon results of previous studies implementing a binary scheme on RGB digital number data alone (Riihimäki et al., 2019).

Due to the single-image width of the orthomosaics used here and the lack of ground control points or Real-Time Kinetic (RTK) data from a high accuracy Global Navigation Satellite System (GNSS) receiver, digital elevation models (DEMs) could not be generated for the UAV sites. The use of such DEMs in the UAV-scale classification could further improve accuracy. The effectiveness of elevation variables and RGB textural information for UAV based vegetation classification is highlighted by Bergamo et al., 2023, using a UAV system similar to that deployed here. While textural information could have been derived from the UAV data used in this study, producing these data is computationally expensive and were therefore excluded. With more computational resources however textural information can be derived from UAV data directly in R using the GLCM package, as in other studies (Bergamo et al., 2023).

The site specific classification accuracy shows low variation, with a range of 6.4% and 0.08 in accuracy and kappa measures, respectively. Other studies which have implemented RGB UAV data for vegetation classification tasks show similar results across a range of environmental

settings (Bergamo et al., 2023; Furukawa et al., 2021; Riihimäki et al., 2019). The low variation in accuracy between sites may be due in part to the site specific model approach taken here. While fitting an individual model for each site is more time consuming compared to fitting a single model across all sites it likely limits the error induced by variations in illumination and weather conditions (Furukawa et al., 2021; Wang et al., 2023). This is an important consideration for implementing these methods across a greater number of UAV sites in regions where weather can change dramatically over short periods, such as in northeastern Iceland. Use of tuning functions, like the grid search from the *caret* package provides the potential for site specific model fitting to be semi-automated.

## 4.2 Upscaling and satellite scale mapping

The upscaling methods implemented here illustrate that the use of UAV data can provide large training and validation sets for building satellite-scale models, as is highlighted in previous studies (Fraser et al., 2017, 2022). From the six UAV sites a total of 12,801 training and 5,487 validation points were generated. Producing a dataset of this size at the resolution of Sentinel-2 imagery via on-foot sampling would be laborious and costly.

The satellite-scale RF regression model shows high overall agreement (R<sup>2</sup> = 0.814) with the UAV based bare soil cover data (Figure 5 & 6a). These results highlight the power of RF regression for estimating fractional coverage of physical parameters across a Sentinel-2 pixel. Previous studies have illustrated the power of RF regression for estimating fractional cover of invasive plant species from satellite data, producing accuracy similar to that shown here (Kattenborn et al., 2019; Shiferaw et al., 2019). While RF regression appears to be a robust model for UAV upscaling, based on these results and those of previous studies, various models

should be examined through more exhaustive performance measures and for variables beyond those related to vegetation (Fraser et al., 2022; Kattenborn et al., 2019)

The site specific regression accuracies show a large range, with R<sup>2</sup> values much lower than the overall value. The lowest R<sup>2</sup> (0.403) was produced at site 400-1 (Figure 6b). Site 400-1 is characterized by a consistent pattern of many small bare soil patches (5 - 20 cm diameter) and a high degree of non-green vegetation cover. The VI's used for the satellite-scale regression model largely rely on the NIR and red bands, as do most widely used VI's. The spectral signature produced by non-green vegetation at these wavelengths is not as easily distinguished from bare soil as green vegetation is (French et al., 2008). This is likely why the model predicts higher bare soil cover at site 400-1 than is shown in the UAV data. The inclusion of shortwave infrared (SWIR) information or indices may improve the performance of the model for non-green vegetation dominated areas. Green and non-green vegetation show increased separability in the 2200 nm range, as such the use of Sentinel-2 band 12 (2190 nm) is recommended in future applications (Amin et al., 2021). Despite the lack of NIR and SWIR information in the UAV data the classification achieved good results in separating bare soil and non-green vegetation for site 400-1 (Table 1). This is likely due to the high resolution of the UAV data, suggesting that increased resolution may be able to improve separability of spectrally similar cover types. Therefore, higher resolution multispectral satellite data, for example PlanteScope (3 m), may better detect non-green vegetation and produce better results.

#### 4.3 Future work

While the fraction of bare soil to vegetation cover over a given area is strongly related in many areas to soil erosion it is not the sole factor (Zhongming et al., 2010). This study has shown UAV

data upscaling to be an effective method for estimating variables related to soil erosion. In addition to improving estimates of bare soil cover, future efforts should investigate additional parameters that may benefit from upscaling.

Related to vegetation cover, vegetation structure is also related to soil erosion. Erosion severity influences, and is influenced by, the types of vegetation present as well as vegetation distribution over a given area (Jiao et al., 2009; Tsuyuzaki & Titus, 1996). Estimating fractional coverage of vegetation such as woody shrub species for example may be useful for soil erosion monitoring and has been successfully upscaled from UAV data using Sentinel-2 data in previous studies. Having an estimate of fractional shrub coverage may also help address issues related to arctic shrubification obscuring soil erosion is satellite data raised by a recent study in Iceland (Kodl et al., 2024).

Producing high resolution DEMs from UAV site data opens the potential for complex structural variables to be derived. Upscaling of canopy metrics using synthetic aperture radar (SAR) data may be useful in further estimating vegetation structure due to the various scattering mechanisms associated with SAR and its application in classifying tundra vegetation (Ullmann et al., 2014). SAR can also be used to estimate surface roughness associated with surface sediment properties in regions with little vegetation cover (Gaber et al., 2015). Using high resolution UAV derived DEMs could provide a method for relating SAR backscatter to surface roughness associated with small scale erosional features (Ullmann & Stauch, 2020).

#### 5.0 Conclusion

This study demonstrates the efficacy of integrating UAV and satellite data to assess physical parameters for mapping and monitoring soil erosion in tundra environments. Using a combination of RF classification and regression models we achieved promising results in estimating bare soil cover and erosion severity at the satellite-scale from UAV data.

The UAV-scale classifications showed high accuracy across all sites despite suboptimal illumination and weather conditions. This highlights the robustness of using multiple VI's and a site specific model approach for classification. Upscaling of the UAV classifications to estimate bare soil cover at the satellite-scale using a RF regression model produced high overall accuracy. However, site specific assessment showed variation in accuracy, indicating underlying land cover conditions may impact results locally. As such, incorporating training data from a wide range of land conditions and cover types would likely improve the applicability of the model. The use of additional spaceborne sensors, such as SAR, as well as UAV derived DEMs should be integrated into this framework as a means for improving erosion characterization. In conclusion the methods and findings presented here illustrate the power and potential of integrating UAV and Satellite data for monitoring soil erosion and land degradation in tundra environments.

## **6.0 References**

- Alvarez-Vanhard, E., Corpetti, T., & Houet, T. (2021). UAV & satellite synergies for optical remote sensing applications: A literature review. *Science of Remote Sensing*, *3*, 100019. https://doi.org/10.1016/j.srs.2021.100019
- Amin, E., Verrelst, J., Rivera-Caicedo, J. P., Pipia, L., Ruiz-Verdú, A., & Moreno, J. (2021).
   Prototyping Sentinel-2 green LAI and brown LAI products for cropland monitoring.
   Remote Sensing of Environment, 255, 112168. https://doi.org/10.1016/j.rse.2020.112168
- Andreatta, D., Gianelle, D., Scotton, M., & Dalponte, M. (2022). Estimating grassland vegetation cover with remote sensing: A comparison between Landsat-8, Sentinel-2 and PlanetScope imagery. *Ecological Indicators*, 141, 109102. https://doi.org/10.1016/j.ecolind.2022.109102
- Arnalds, O. (2015). *The Soils of Iceland*. Springer Netherlands. https://doi.org/10.1007/978-94-017-9621-7
- Arnalds, O., & Barkarson, B. H. (2003). Soil erosion and land use policy in Iceland in relation to sheep grazing and government subsidies. *Environmental Science & Policy*, *6*(1), 105–113. https://doi.org/10.1016/S1462-9011(02)00115-6
- Arnalds, O., Ísland, & Rannsóknastofnun Landbunaðarins (Eds.). (2001). *Soil erosion in Iceland*. Soil Conservation Service.
- Arnalds, Ó., Marteinsdóttir, B., Brink, S. H., & Þórsson, J. (2023). A framework model for current land condition in Iceland. *PLOS ONE*, 18(7), e0287764. https://doi.org/10.1371/journal.pone.0287764
- Arnalds, O., & Óskarsson, H. (2009). A soil map of Iceland. Nátturufraedingurinn, 78, 107–121.

- Ayalew, D. A., Deumlich, D., Šarapatka, B., & Doktor, D. (2020). Quantifying the Sensitivity of NDVI-Based C Factor Estimation and Potential Soil Erosion Prediction using Spaceborne Earth Observation Data. *Remote Sensing*, *12*(7), Article 7. https://doi.org/10.3390/rs12071136
- Bergamo, T. F., de Lima, R. S., Kull, T., Ward, R. D., Sepp, K., & Villoslada, M. (2023). From UAV to PlanetScope: Upscaling fractional cover of an invasive species Rosa rugosa. *Journal of Environmental Management*, 336, 117693.

  https://doi.org/10.1016/j.jenvman.2023.117693
- Borrelli, P., Alewell, C., Alvarez, P., Anache, J. A. A., Baartman, J., Ballabio, C., Bezak, N.,
  Biddoccu, M., Cerdà, A., Chalise, D., Chen, S., Chen, W., De Girolamo, A. M., Gessesse,
  G. D., Deumlich, D., Diodato, N., Efthimiou, N., Erpul, G., Fiener, P., ... Panagos, P.
  (2021). Soil erosion modelling: A global review and statistical analysis. *Science of The Total Environment*, 780, 146494. https://doi.org/10.1016/j.scitotenv.2021.146494
- Boulanger-Lapointe, N., Ágústsdóttir, K., Barrio, I. C., Defourneaux, M., Finnsdóttir, R., Jónsdóttir, I. S., Marteinsdóttir, B., Mitchell, C., Möller, M., Nielsen, Ó. K., Sigfússon, A. Þ., Þórisson, S. G., & Huettmann, F. (2022). Herbivore species coexistence in changing rangeland ecosystems: First high resolution national open-source and open-access ensemble models for Iceland. *Science of The Total Environment*, 845, 157140. https://doi.org/10.1016/j.scitotenv.2022.157140
- Buchhorn, M., Walker, D. A., Heim, B., Raynolds, M. K., Epstein, H. E., & Schwieder, M.
  (2013). Ground-Based Hyperspectral Characterization of Alaska Tundra Vegetation along
  Environmental Gradients. *Remote Sensing*, 5(8), Article 8.
  https://doi.org/10.3390/rs5083971

- Dugmore, A. J., Gisladóttir, G., Simpson, I. A., & Newton, A. (2009). Conceptual Models of 1200 Years of Icelandic Soil Erosion Reconstructed Using Tephrochronology. *Journal of the North Atlantic*, *2*(1), 1–18. https://doi.org/10.3721/037.002.0103
- Durán Zuazo, V. H., Rodríguez Pleguezuelo, C. R., Francia Martínez, J. R., Cárceles Rodríguez, B., Martínez Raya, A., & Pérez Galindo, P. (2008). Harvest intensity of aromatic shrubs vs. soil erosion: An equilibrium for sustainable agriculture (SE Spain). *CATENA*, 73(1), 107–116. https://doi.org/10.1016/j.catena.2007.09.006
- Fernández, D., Adermann, E., Pizzolato, M., Pechenkin, R., & Rodríguez, C. G. (2022).

  REMOTE MAPPING OF SOIL EROSION RISK IN ICELAND. *The International Archives of the Photogrammetry, Remote Sensing and Spatial Information Sciences*, XLVIII-4-W1-2022, 135–141.

  https://doi.org/10.5194/isprs-archives-XLVIII-4-W1-2022-135-2022
- Fraser, R. H., Pouliot, D., & van der Sluijs, J. (2022). UAV and High Resolution Satellite

  Mapping of Forage Lichen (Cladonia spp.) in a Rocky Canadian Shield Landscape.

  Canadian Journal of Remote Sensing, 48(1), 5–18.

  https://doi.org/10.1080/07038992.2021.1908118
- Fraser, R. H., Van der Sluijs, J., & Hall, R. J. (2017). Calibrating Satellite-Based Indices of Burn Severity from UAV-Derived Metrics of a Burned Boreal Forest in NWT, Canada. *Remote Sensing*, *9*(3), Article 3. https://doi.org/10.3390/rs9030279
- French, A. N., Schmugge, T. J., Ritchie, J. C., Hsu, A., Jacob, F., & Ogawa, K. (2008). Detecting land cover change at the Jornada Experimental Range, New Mexico with ASTER emissivities. *Remote Sensing of Environment*, *112*(4), 1730–1748. https://doi.org/10.1016/j.rse.2007.08.020

- Furukawa, F., Laneng, L. A., Ando, H., Yoshimura, N., Kaneko, M., & Morimoto, J. (2021).
  Comparison of RGB and Multispectral Unmanned Aerial Vehicle for Monitoring
  Vegetation Coverage Changes on a Landslide Area. *Drones*, 5(3), Article 3.
  https://doi.org/10.3390/drones5030097
- Gaber, A., Soliman, F., Koch, M., & El-Baz, F. (2015). Using full-polarimetric SAR data to characterize the surface sediments in desert areas: A case study in El-Gallaba Plain, Egypt. *Remote Sensing of Environment*, *162*, 11–28. https://doi.org/10.1016/j.rse.2015.01.024
- Gitelson, A. A., Kaufman, Y. J., Stark, R., & Rundquist, D. (2002). Novel algorithms for remote estimation of vegetation fraction. *Remote Sensing of Environment*, 80(1), 76–87. https://doi.org/10.1016/S0034-4257(01)00289-9
- Greipsson, S. (2012). Catastrophic soil erosion in Iceland: Impact of long-term climate change, compounded natural disturbances and human driven land-use changes. *CATENA*, *98*, 41–54. https://doi.org/10.1016/j.catena.2012.05.015
- Guijarro, M., Pajares, G., Riomoros, I., Herrera, P. J., Burgos-Artizzu, X. P., & Ribeiro, A.
   (2011). Automatic segmentation of relevant textures in agricultural images. *Computers and Electronics in Agriculture*, 75(1), 75–83.
   https://doi.org/10.1016/j.compag.2010.09.013
- Gyssels, G., Poesen, J., Bochet, E., & Li, Y. (2005). Impact of plant roots on the resistance of soils to erosion by water: A review. *Progress in Physical Geography: Earth and Environment*, 29(2), 189–217. https://doi.org/10.1191/0309133305pp443ra
- Harmse, C. J., Gerber, H., & van Niekerk, A. (2022). Evaluating Several Vegetation Indices

  Derived from Sentinel-2 Imagery for Quantifying Localized Overgrazing in a Semi-Arid

- Region of South Africa. *Remote Sensing*, *14*(7), Article 7. https://doi.org/10.3390/rs14071720
- Hijmans, R. J. (2023). terra: Spatial Data Analysis. https://CRAN.R-project.org/package=terra
- Hurcom, S. J., & Harrison, A. R. (1998). The NDVI and spectral decomposition for semi-arid vegetation abundance estimation. *International Journal of Remote Sensing*, 19(16), 3109–3125. https://doi.org/10.1080/014311698214217
- Icelandic Meteorological Office. (2012). *Climatological data*. Icelandic Meteorological Office. https://en.vedur.is/climatology/data/
- Jiao, J., Zou, H., Jia, Y., & Wang, N. (2009). Research progress on the effects of soil erosion on vegetation. *Acta Ecologica Sinica*, 29(2), 85–91. https://doi.org/10.1016/j.chnaes.2009.05.001
- Juszak, I., Erb, A. M., Maximov, T. C., & Schaepman-Strub, G. (2014). Arctic shrub effects on NDVI, summer albedo and soil shading. *Remote Sensing of Environment*, 153, 79–89. https://doi.org/10.1016/j.rse.2014.07.021
- Kardjilov, M. I., Gisladottir, G., & Gislason, S. R. (2006). Land degradation in northeastern Iceland: Present and past carbon fluxes. *Land Degradation & Development*, *17*(4), 401–417. https://doi.org/10.1002/ldr.746
- Kattenborn, T., Lopatin, J., Förster, M., Braun, A. C., & Fassnacht, F. E. (2019). UAV data as alternative to field sampling to map woody invasive species based on combined Sentinel-1 and Sentinel-2 data. *Remote Sensing of Environment*, 227, 61–73. https://doi.org/10.1016/j.rse.2019.03.025
- Knipling, E. B. (1970). Physical and physiological basis for the reflectance of visible and near-infrared radiation from vegetation. *Remote Sensing of Environment*, 1(3), 155–159.

- https://doi.org/10.1016/S0034-4257(70)80021-9
- Kodl, G., Streeter, R., Cutler, N., & Bolch, T. (2024). Arctic tundra shrubification can obscure increasing levels of soil erosion in NDVI assessments of land cover derived from satellite imagery. *Remote Sensing of Environment*, 301, 113935.
  https://doi.org/10.1016/j.rse.2023.113935
- Kuhn & Max. (2008). Building Predictive Models in R Using the caret Package. *Journal of Statistical Software*, 28(5), 1–26. https://doi.org/10.18637/jss.v028.i05
- Laidler, G. J., Treitz, P. M., & Atkinson, D. M. (2008). Remote Sensing of Arctic Vegetation:

  Relations between the NDVI, Spatial Resolution and Vegetation Cover on Boothia

  Peninsula, Nunavut. *Arctic*, *61*(1), 1–13.
- Liaw, A., & Wiener, M. (2002). Classification and Regression by randomForest. *R News*, *2*(3), 18–22.
- Liu, N., Budkewitsch, P., & Treitz, P. (2017). Examining spectral reflectance features related to Arctic percent vegetation cover: Implications for hyperspectral remote sensing of Arctic tundra. *Remote Sensing of Environment*, 192, 58–72. https://doi.org/10.1016/j.rse.2017.02.002
- Main-Knorn, M., Pflug, B., Louis, J., Debaecker, V., Müller-Wilm, U., & Gascon, F. (2017).

  Sen2Cor for Sentinel-2. *Image and Signal Processing for Remote Sensing XXIII*, 10427, 37–48. https://doi.org/10.1117/12.2278218
- Marcial-Pablo, M. de J., Gonzalez-Sanchez, A., Jimenez-Jimenez, S. I., Ontiveros-Capurata, R.
  E., & Ojeda-Bustamante, W. (2019). Estimation of vegetation fraction using RGB and multispectral images from UAV. *International Journal of Remote Sensing*, 40(2), 420–438. https://doi.org/10.1080/01431161.2018.1528017

- Marteinsdóttir, B., Þórarinsdóttir, E., Halldórsson, G., Stefánsson, J., Þórsson, J., Svavarsdóttir, K., Finnsdóttir, R., & Jónsdóttir, S. (2021). GróLind Sustainable Land Use Based on Ecological Knowledge. *IGC Proceedings (2001-2023)*. https://uknowledge.uky.edu/igc/24/1/25
- McGovern, T. H., Vésteinsson, O., Fridriksson, A., Church, M., Lawson, I., Simpson, I. A.,
  Einarsson, A., Dugmore, A., Cook, G., Perdikaris, S., Edwards, K. J., Thomson, A. M.,
  Adderley, W. P., Newton, A., Lucas, G., Edvardsson, R., Aldred, O., & Dunbar, E.
  (2007). Landscapes of Settlement in Northern Iceland: Historical Ecology of Human
  Impact and Climate Fluctuation on the Millennial Scale. *American Anthropologist*,
  109(1), 27–51. https://doi.org/10.1525/aa.2007.109.1.27
- Meyer, G. E., & Neto, J. C. (2008). Verification of color vegetation indices for automated crop imaging applications. *Computers and Electronics in Agriculture*, 63(2), 282–293. https://doi.org/10.1016/j.compag.2008.03.009
- Myers-Smith, I. H., Kerby, J. T., Phoenix, G. K., Bjerke, J. W., Epstein, H. E., Assmann, J. J.,
  John, C., Andreu-Hayles, L., Angers-Blondin, S., Beck, P. S. A., Berner, L. T., Bhatt, U.
  S., Bjorkman, A. D., Blok, D., Bryn, A., Christiansen, C. T., Cornelissen, J. H. C.,
  Cunliffe, A. M., Elmendorf, S. C., ... Wipf, S. (2020). Complexity revealed in the
  greening of the Arctic. *Nature Climate Change*, 10(2), Article 2.
  https://doi.org/10.1038/s41558-019-0688-1
- Ólafsdóttir, R., Schlyter, P., & Haraldsson, H. V. (2001). Simulating Icelandic Vegetation Cover during the Holocene Implications for Long-Term Land Degradation. *Geografiska Annaler. Series A, Physical Geography*, 83(4), 203–215.
- Poesen, J. (2018). Soil erosion in the Anthropocene: Research needs. Earth Surface Processes

- and Landforms, 43(1), 64–84. https://doi.org/10.1002/esp.4250
- QGIS Development Team. (2009). *QGIS Geographic Information System* [Computer software].

  Open Source Geospatial Foundation. http://qgis.org
- R Core Team. (2022). *R: A Language and Environment for Statistical Computing* [Computer software]. R Foundation for Statistical Computing. https://www.R-project.org/
- Riihimäki, H., Luoto, M., & Heiskanen, J. (2019). Estimating fractional cover of tundra vegetation at multiple scales using unmanned aerial systems and optical satellite data.

  \*Remote Sensing of Environment, 224, 119–132. https://doi.org/10.1016/j.rse.2019.01.030
- Sentinel-2 Global Mosaic service. (2014). https://s2gm.land.copernicus.eu/
- Sepuru, T. K., & Dube, T. (2018). An appraisal on the progress of remote sensing applications in soil erosion mapping and monitoring. *Remote Sensing Applications: Society and Environment*, *9*, 1–9. https://doi.org/10.1016/j.rsase.2017.10.005
- Shiferaw, H., Bewket, W., & Eckert, S. (2019). Performances of machine learning algorithms for mapping fractional cover of an invasive plant species in a dryland ecosystem. *Ecology* and *Evolution*, *9*(5), 2562–2574. https://doi.org/10.1002/ece3.4919
- Streeter, R. T., & Cutler, N. A. (2020). Assessing spatial patterns of soil erosion in a high-latitude rangeland. *Land Degradation & Development*, 31(15), 2003–2018. https://doi.org/10.1002/ldr.3585
- Tang, C., Liu, Y., Li, Z., Guo, L., Xu, A., & Zhao, J. (2021). Effectiveness of vegetation cover pattern on regulating soil erosion and runoff generation in red soil environment, southern China. *Ecological Indicators*, *129*, 107956. https://doi.org/10.1016/j.ecolind.2021.107956
- Thórhallsdóttir. (1997). Tundra ecosystems of Iceland. *Ecosystems of the World: Polar and Alpine Tundra*, 152–163.

- Tsuyuzaki, S., & Titus, J. H. (1996). Vegetation development patterns in erosive areas on the pumice plains of Mount St. Helens: American Midland Naturalist. *American Midland Naturalist*, *135*, 172–177. https://doi.org/10.2307/2426883
- Ullmann, T., Schmitt, A., Roth, A., Duffe, J., Dech, S., Hubberten, H.-W., & Baumhauer, R.
  (2014). Land Cover Characterization and Classification of Arctic Tundra Environments
  by Means of Polarized Synthetic Aperture X- and C-Band Radar (PolSAR) and Landsat 8
  Multispectral Imagery—Richards Island, Canada. *Remote Sensing*, 6(9), Article 9.
  https://doi.org/10.3390/rs6098565
- Ullmann, T., & Stauch, G. (2020). Surface Roughness Estimation in the Orog Nuur Basin (Southern Mongolia) Using Sentinel-1 SAR Time Series and Ground-Based Photogrammetry. *Remote Sensing*, *12*(19), Article 19. https://doi.org/10.3390/rs12193200
- Vieira, A., & Rodrigues, S. C. (2021). *Soil Erosion: Current Challenges and Future Perspectives* in a Changing World. BoD Books on Demand.
- Virtanen, T., & Ek, M. (2014). The fragmented nature of tundra landscape. *International Journal of Applied Earth Observation and Geoinformation*, *27*, 4–12. https://doi.org/10.1016/j.jag.2013.05.010
- Wang, Y., Yang, Z., Kootstra, G., & Khan, H. A. (2023). The impact of variable illumination on vegetation indices and evaluation of illumination correction methods on chlorophyll content estimation using UAV imagery. *Plant Methods*, 19(1), 51.
  https://doi.org/10.1186/s13007-023-01028-8
- Xiao, J., & Moody, A. (2005). A comparison of methods for estimating fractional green vegetation cover within a desert-to-upland transition zone in central New Mexico, USA.

  \*Remote Sensing of Environment, 98(2), 237–250.

https://doi.org/10.1016/j.rse.2005.07.011

Zhongming, W., Lees, B. G., Feng, J., Wanning, L., & Haijing, S. (2010). Stratified vegetation cover index: A new way to assess vegetation impact on soil erosion. *CATENA*, *83*(1), 87–93. https://doi.org/10.1016/j.catena.2010.07.006

# Appendix

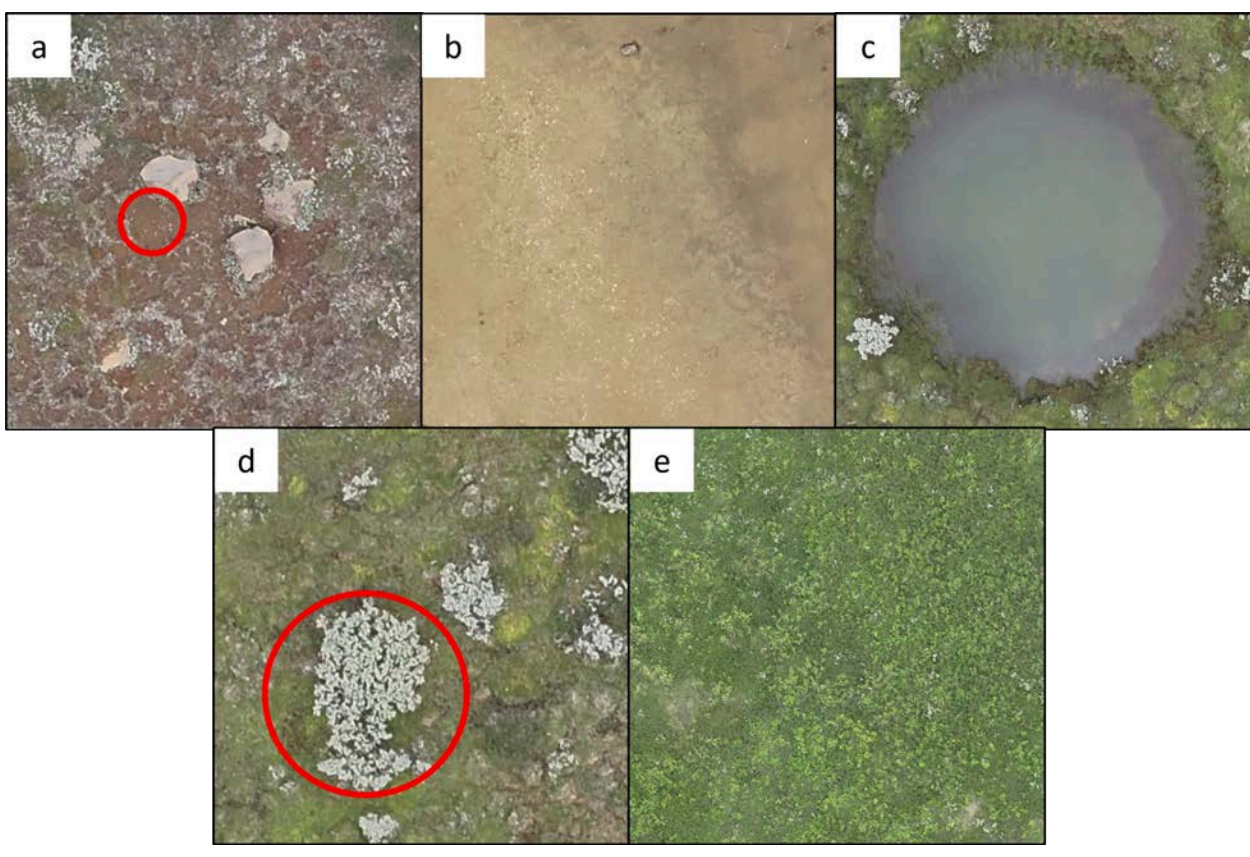


Figure A1: Examples of class types used in the UAV-scale classification. a) Bare soil (dark), b) bare soil (light), c) water, d) non-green vegetation, e) green vegetation. Specific examples for a and d are highlighted with red circles.